Journal of Thermal Analysis and Calorimetry
https://doi.org/10.1007/s10973-025-13994-3

Experimental investigation of the thermal and hydrodynamic performances of plate-fin heat exchangers (PFHE) using MgO–water nanofluid as an enhanced coolant

Fatih Aktas[1] · Emre Askin Elibol[2] · Aleyna Eda Aksoy[1] · Diren Deniz Cicek[1,3] · Muhammed Ali Oztemel[1] · Didem Cetin[1] · Oguz Turgut[1]

Received: 10 October 2024 / Accepted: 5 January 2025
© The Author(s) 2025

Abstract
Plate-fin heat exchangers (PFHEs) are commonly employed in automobile applications as radiators and play a vital role in waste heat management. The performance of common coolants for this type of heat exchangers can be enhanced by incorporating nanofluids as coolants. In this study, the coolant of MgO–pure water nanofluids having different nanoparticle volume concentrations have been utilized for a PFHE having offset-strip fins for coolant side and wavy fins for air side. The effects of different inlet temperatures of 40, 50, 60, 70, and 80 °C and coolant flow rates of 5, 8, and 11 LPM and different nanoparticle volume concentrations of 0, 0.025, 0.05, 0.1, and 0.2% on the thermo-hydraulic behavior of radiator were investigated. The Reynolds number, heat transfer coefficient, heat transfer rate, Nusselt number and pressure drop have been taken into account as output parameters of the experiments. It has been concluded that there is a critical value for nanoparticle volume concentration (0.025%) at which the Reynolds number, heat transfer rate, heat transfer coefficient and Nu number reaches its maximum values. For instance, at a nanoparticle volume concentration of 0.025%, an increase of 265% was observed as the inlet temperature increased from 40 to 80 °C at a flow rate of 11 LPM. The maximum Reynolds number was also observed at this nanoparticle volume concentration for all tested flow rates and inlet temperatures. As for the pressure drop, increasing the nanoparticle volume concentration resulted in a rise in pressure drop across the radiator, with the highest value recorded at a 0.2% concentration. A noticeable reduction in pumping power was observed at higher inlet temperatures for a fixed flow rate and nanoparticle concentration. These findings indicate that the use of MgO–pure water nanofluids with an optimal nanoparticle concentration (0.025%) can substantially enhance the thermal and hydraulic performance of PFHEs in automotive radiator applications.

Keywords Plate-fin heat exchanger · Radiator · Fin · Nanofluid · MgO nanoparticle

Introduction

Plate-fin heat exchangers (PFHEs) are crucial components in industrial applications requiring efficient heat transfer. Automobile radiators are one example of an application considering waste heat management. In such applications, compactness is a critical feature, as space is limited by the engine and other components. PFHEs are classified as compact heat exchangers that can be utilized in such applications owing to its extended heat transfer area. Such a device's cooling capability is important since it directly impacts the engine's performance and lifespan. Because of the channel geometry, these types of heat exchangers also exhibit high thermal and hydraulic performance which makes it suitable for automobile radiators. According to Kays and London

✉ Fatih Aktas
fatihaktas@gazi.edu.tr

[1] Department of Mechanical Engineering, Faculty of Engineering, Gazi University, 06570 Maltepe, Ankara, Türkiye

[2] Department of Mechanical Engineering, Faculty of Engineering, Giresun University, 28200 Merkez, Giresun, Türkiye

[3] Graduate School of Natural and Applied Sciences, Gazi University, 06500 Yenimahalle, Ankara, Türkiye

Published online: 31 January 2025

identifications, there are four fundamental channel geometry of PFHEs: plain fin, perforated fin, wavy fin, and offset-strip fin (OSF) [1]. The periodical disruption of the thermal boundary layer enhances heat transport, facilitated by the OSF configuration. The intermittent disruption enhances heat transport by inhibiting the formation of the thermal boundary layer. As to wavy fins, heat transfer improves by secondary flows which result in flow separation throughout the channel.

Because of the versatility of applications and high efficiency feature of PFHEs [2, 3], many researchers have studied this subject. In the study of Yang et al. [4] heat transfer behavior of PFHE with OSF has experimentally been investigated. Total of 18 different fin configurations using the coolant of pure water have been studied. As a result of the findings, new correlation for Colburn factor has been proposed. The study of Blecich et al. [5] investigates the thermo-hydraulic performance of PFHEs having OSF numerically. Fin-by-fin analyses have shown that interrupting the thermal boundary layer, which is a consequence of the OSF structure, enhances the heat transfer behavior of the fins. Authors also have studied the effect of the fin thickness on the thermo-hydraulic behavior, and it has been concluded that lowering the fin thickness increases the efficiency. The study conducted by Xiang et al. [6] investigated the effect of various offsets on the thermal and hydraulic performance of a PFHE numerically. The new correlations have been proposed for pure water with the help of regression analyses.

Although PFHEs have high heat transfer performance, vehicle radiators using nanofluids rather than pure water can achieve even greater heat transfer [7–10]. For this reason, numerous research has been done in the literature that examine using nanofluid as radiator coolant in place of pure water. Choi [11] was the first researcher who claimed that the thermal conductivity of a fluid can be increased by adding nanoparticles with a diameter of 1–100 nm so that the resulting fluid is called nanofluid which has superior thermophysical properties. Therefore, utilization of nanofluids as coolant in PFHEs has been the subject of numerous investigations conducted by many researchers. Aliabadi and Salami [12] have studied the thermal and hydraulic performance of a PFHE having OSF configuration and varying fin parameters. Al_2O_3–water nanofluid has been utilized throughout the numerical study. The effect of Al_2O_3 volume concentration (φ) which varies from 0.1 to 0.5% has been observed. The authors concluded that the efficacy of the PFHE is enhanced as the φ rises. The study conducted by Kumar et al. [13] employed a hybrid nanofluid consisting of multiwall carbon nanotube-SiO_2-Ethylene Glycol–water as a coolant in a vehicle radiator with louvered fins. The cooling performance of this nanofluid was observed by experimental methods. Experimental results demonstrated that the hybrid nanofluid outperformed conventional base fluids for all flow rates and external air velocities. The work of Karana and Sahoo [14] focuses on the theoretical investigation of the performance of thermoelectric generators. Specifically, they examine the use of ethylene glycol MgO and ZnO nanofluids as coolants in the waste heat recovery system of automobiles. The authors stated that using ethylene glycol MgO instead of ZnO nanoparticle can enhance the power output and circuit voltage of the thermoelectric generator, while keeping all other conditions identical. The work conducted by Rai et al. [15] utilized water–MgO nanofluid as a coolant for vehicle radiators. The purpose was to experimentally explore the impact of various flow rates and inlet temperatures of the coolant on heat transfer enhancement. The study has determined that the increase of mass flow rate and introducing MgO nanoparticles have enhanced the rate of heat transfer. The study conducted by Ali et al. [16] examines the thermal management of an automobile radiator using water–MgO nanofluid as a coolant with varying φ of 0.06%, 0.09%, and 0.12%. The experimental findings indicate that the heat transfer was improved when compared to the pure base fluid. A maximum improvement of 31% was observed at a φ of 0.12% MgO. In the study of Gamal et al. [17] heat transfer performance of a flat tube automobile radiator using the coolant of water/ethylene glycol MgO and ZnO nanofluid has been investigated numerically for the Reynolds number range of 250–1750. Various nanoparticle volume fractions (φ) were studied. It has been observed that the compared to base fluids, the heat transfer coefficient is enhanced 17.1% and 13.4% for MgO and ZnO nanofluids, respectively. The study of Kadam et al. [18] focuses on the heat transfer enhancement by utilizing MgO–water nanofluid flowing through tube. Authors have examined the effects of different φ on the heat transfer coefficient experimentally. As a result, they have found that the heat transfer augmentation enhances as the φ increases. The study conducted by Hamzah and Al-Amir [19] experimentally investigates the effects of introducing MgO nanoparticles to pure water with six different φ values which is a coolant fluid for automobile radiators. It has been concluded that adding MgO nanoparticles to pure water increases the heat transfer rate of the vehicle radiator for all φ values compared to pure water. Li et al. [20] numerically investigated the hydrothermal behavior of the MgO–Ag/water hybrid nanofluid for sinusoidal hairpin heat exchanger. It has been observed that, between the Reynolds number of 100–500, increasing the nanoparticle volume concentration has increased the irreversibility. On the other hand, between the Reynolds number of 1000 and 1500 the opposite has been observed. Also, it has been concluded that the increasing either Reynolds number or nanoparticle volume concentration has shown a positive effect on the heat transfer rate and total heat transfer coefficient. Jasim et al. [21] has investigated the hydrothermal behavior of the shell and helical coil tube heat exchanger

with MgO–TiO_2/water nanofluid numerically. It has been concluded that the increasing Reynolds number has a positive effect on the both heat transfer, Nusselt number values, and heat transfer efficiency. Azizi et al. [22] have numerically investigated the hydrothermal behavior of the shell and conical coil tube heat exchanger utilizing MgO–TiO_2/water nanofluid. The effect of the Dean number on the thermal performance has been evaluated and it has been concluded that at the same nanoparticle volume concentrations, there is a critical value of Dean number in which the thermal performance is maximum.

A review of the literature reveals several studies focusing on the thermo-hydraulic behavior of heat exchangers using MgO-based nanofluids. However, most of these works center on shell-and-coil heat exchangers or similar configurations. Different from the literature, the thermo-hydraulic behavior of the plate fin heat exchanger with MgO/water nanofluid has been investigated experimentally, which has not been considered in the literature before. The purpose of this work is to examine at the thermal and hydrodynamic behavior of plate-fin heat exchangers (PFHE) specifically built for automotive applications, employing MgO–pure water nanofluid as a novel coolant. Unlike conventional coolants, the use of MgO–pure water nanofluid in PFHEs, particularly with offset-strip fins (OSF) on the coolant side and wavy fins on the air side, is a new technique in the literature. This novel arrangement and nanofluid selection offer new perspectives into improving heat transfer performance in vehicle cooling systems. An experimental investigation was conducted to examine the effects of important parameters—such as the volume fraction (φ) of nanoparticles, coolant inlet temperature, and volume flow rate—on the thermal and hydrodynamic performance of the system. By addressing this previously unexamined combination of coolant and fin geometry, the study contributes a distinctive perspective to the field of heat exchanger technology.

Experimental

In this section experimental procedure has been explained and some basic equations for calculation of the thermal and hydrodynamic parameters are presented.

Nanofluid preparation

MgO nanoparticle utilized in this investigation was obtained from NANOGRAFI business and has an 18 nm diameter. The mean diameter and distribution of nanoparticles provided by corporation are displayed in Fig. 1, which was captured using the scanning electron microscopy (SEM) method at a voltage of acceleration of 30 kV. The figure indicates

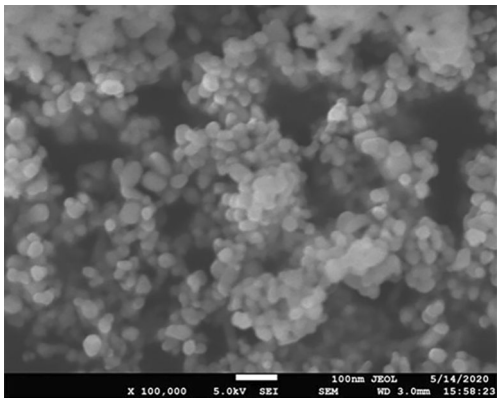


Fig. 1 SEM image of MgO nanoparticles

Table 1 Nanoparticle properties

Characteristics	MgO
Approximate size	18/nm
Thermal conductivity	30/W·m^{-1}·K^{-1}
Purity	99.95/%
Morphology	Spherical
Density	3580/kg m^{-3}
Color	White
Specific heat	877/J kg^{-1} K

that the spherical form of MgO nanoparticles can be considered their overall geometric structure.

The surfactant (Triton X-100) was added to the base fluid during nanofluid preparation process in order to create steady nanofluid distributions. Stabilizing the solution by adding an amount of surfactant determines if the final nanofluid will adapt to the application [23, 24]. It should not be overlooked, nonetheless, because using too much surfactant might lead to nanoparticles sedimenting since they will group together [25]. Additionally, the previously described sedimentation phenomenon lowers the concentration of suspended nanoparticles in suspension, which worsens thermal performance [26]. The problem of accumulation that results from nanoparticles may be mitigated, producing a more stable nanofluid, by integrating of surfactants into the suspension [27]. It is also well known that Triton X-100, with its nonionic and viscous nature, lowers surface tension [28]. The preparation of the nanofluid was done in two steps. All of the characteristics of nanoparticles are listed in Table 1.

Figure 2 depicts the nanofluid's preparation. Ten beakers, each holding one liter, were needed to create a 10-L nanofluid sample. Initially, sensitive weight measurements were made of MgO nanoparticles at φ of 0.025, 0.05, 0.1, and 0.2%. Next, using a magnetic stirrer, the required amount of nanoparticle was added to ten liters of pure water and

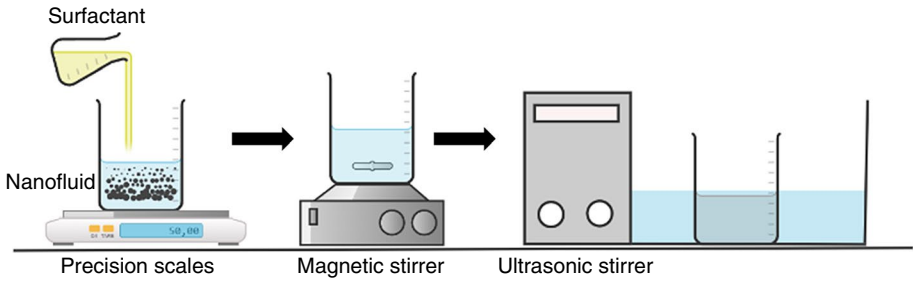


Fig. 2 Preparation of the MgO–pure water nanofluid

agitated for two hours to ensure uniform dispersion. After that, an ultrasonic bath is used to ultrasonically treat the obtained mixture. A crucial element in breaking apart agglomerates is the proper duration of sonication [29]. Since it is known that the sonication time providing the best stability is determined to be 2.5 h [30], this condition has been adopted for the stable suspension of MgO nanoparticles in pure water.

The following equation was utilized to determine the necessary quantity of nanoparticles for the intended φ:

$$\varphi = \left(\frac{\frac{m_p}{\rho_p}}{\frac{m_p}{\rho_p} + \frac{m_{bf}}{\rho_{bf}}} \right) \quad (1)$$

where the sub-indices p and bf denote the particle and the base fluid, respectively.

Experimental setup and procedure

An illustration of the experimental setup for this inquiry, which comprised a fan and radiator, is depicted in Fig. 3. The hot fluid (MgO–water nanofluid) and the cold fluid (air) are the two types of circuits in the experimental setup.

The radiator cools the nanofluid by forcefully forcing air into it using an axial fan. Before being distributed into the circulation, the nanofluid is heated to the required stable inlet temperature using a temperature indicator and controller in the heating tank—the first section of hot fluid circulation. The thirty-liter heating tank is split in two halves. The chilled fluid that is going back into the tank is first heated in a partition with a power resistance of 1 kW. Two 2 kW power resistances are located throughout the remaining portion. Turbine flow meter, a solenoid vane, and a centrifugal pump with three distinct fixed-speed settings are other components of the hot flow system. T-type thermocouples were placed to monitor the temperature of the nanofluid at the radiator's input and exit. Two precise pressure gauges are placed to the radiator's input and output in order to estimate the pressure decrease. An accuracy of ± 0.2 °C was achieved by fixing nine T-type thermocouples at different radiator wall locations to measure the average wall temperature inside the HE core. An Agilent data logger connected to thermocouples was used to record temperature values. A flow meter serves to measure the volume flow rate when fluid is expelled from the tank using a centrifugal pump with a flow rate ranging from 5 to 11 LPM. The ventilation fan sustains a consistent average input air velocity of 2.77 m s^{-1}. The design of the radiator employs an OSF channel for the air flank that is corrugated or wavy, and a rectangular cross section for the nanofluid flank. Figure 4 demonstrates the notations for fin parameters.

The aluminum alloy 3003-H14 is used to produce each fin channel on the radiator. The radiator and fin channel shapes of a large vehicle are seen in Fig. 5. Also, the PFHE with indirect and crossflow arrangement seen in large automobile radiators is shown in Fig. 5.

Table 2 presents the geometrical characteristics of the fin channels. The geometric properties for OSF and wavy fin channels of the HE are shown in Table 2, which is in accordance with the research of Elibol and Turgut [30]. Factors examined and held constant during experiment are listed in

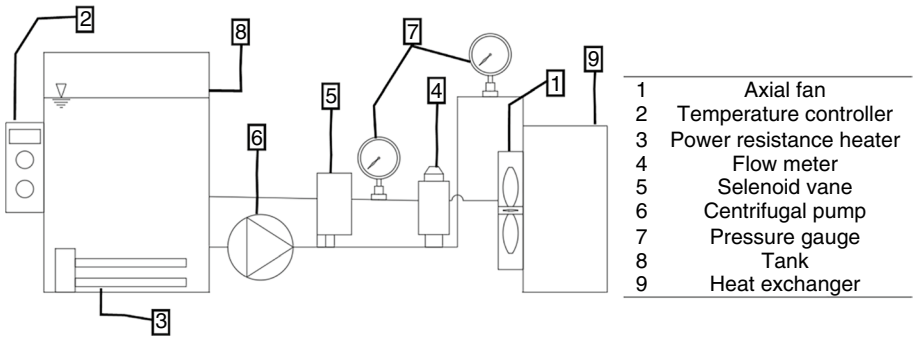


Fig. 3 Demonstration of the experimental setup

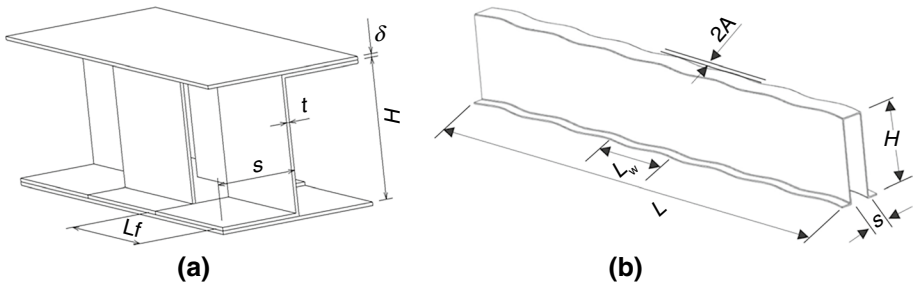


Fig. 4 Notations of fin parameters for: **a** OSF, and **b** Wavy fin

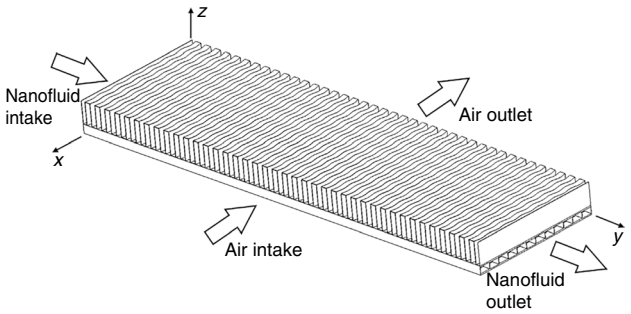


Fig. 5 Section view of radiator shape with wavy fin for air side and OSF for nanofluid side

Table 2 Fin channel geometric parameters

Specifications	Values/mm	
	OSF	Wavy fin
Fin thickness, t	0.15	0.15
Fin length, L_f	3.5	–
Fin height, H	2.85	9.7
Fin space, s	5	2.5
Channel length, L	213.5	62.7
Twice of wavy fin amplitude, 2A	–	0.7
Wave length, L_w	–	11
Top–bottom plate thickness, δ	0.5	0.5

Table 3 Investigative variables: constants and variables

Parameters	Variation
φ/%	0, 0.025, 0.05, 0.1 & 0.2
Inlet temperature of the nanofluid/°C	40, 50, 60, 70 & 80
Volume flow rate of the nanofluid (LPM)	5, 8, 11
Velocity of the air inlet/m s^{-1}	2.77

Table 3. The optimum operating temperatures of heavy vehicle radiators vary between 80 and 100 °C [31]. In this study, the effects of different MgO nanoparticles and volumetric flow rates on the flow characteristics and thermal performance at different temperature values until the cooling water reaches the optimum operating conditions were investigated. The φ is kept low to reduce chance of precipitation, accumulation, aggregation, and pumping issues. When working fluid in the heating tank reaches proper inlet temperature (after the required flow rate has been established), radiator fan and the pump are turned on simultaneously. To make sure the system is stable, experimental configuration is run for thirty minutes.

Nanofluid physical properties

Dispersed evenly throughout the base fluid, deionized water, are MgO nanoparticles. Base fluid, nanofluid, and nanoparticle are represented by the subscriptions b_f, n_f, and p, respectively, while the φ of the nanoparticle is indicated by φ. As a result, the nanofluids' density (ρ_{nf}) and specific heat capacity ($c_{p,nf}$) are calculated as [33].

$$\rho_{nf} = \varphi_p \rho_p + (1 - \varphi_p)\rho_{bf} \tag{2}$$

$$c_{p,nf} = \frac{[\varphi_p \rho_p c_{p,p} + (1 - \varphi_p)\rho_{bf} c_{p,bf}]}{\rho_{nf}} \tag{3}$$

By taking into consideration the diameter and interfacial layer of the nanoparticles, a relatively new work [34] adjusted the usual Maxwell model to determine the nanofluid's thermal conductivity. The φ values in this research was kept low to adhere to the Maxwell model. With the nanoparticles moving in minimal Brownian motion, the thermal conductivity of nanofluid, denoted as k_{nf}, may be calculated using the below formula [35]:

$$k_{nf} = k_{bf} \frac{(k_p + 2k_{bf}) - 2\varphi_p(k_{bf} - k_p)}{(k_p + 2k_{bf}) + \varphi_p(k_{bf} - k_p)} \tag{4}$$

The below formula [36] can be employed to ascertain the viscosity of nanofluid:

$$\mu_{nf} = \frac{\mu_{bf}}{1 - 34.87(d_p/d_{bf})^{-0.3} \varphi_p^{1.03}} \tag{5}$$

$$d_{bf} = \left(\frac{6M}{N\pi\rho_{bf0}}\right)^{1/3} \tag{6}$$

Where by M is basic fluid's molecular weight. The dimension is d, the base fluid density is estimated at 293 K, and the Avogadro number is N.

Data reduction

An approach may be used to determine the average Nusselt number, average heat transfer rate, and average heat transfer coefficient for the nanofluid side. Equation (7) clarifies how to calculate the nanofluid's heat transfer rate by conserving mass and energy.

$$\dot{Q} = \dot{m}c_{\mathrm{p}}(T_{\mathrm{in}} - T_{\mathrm{out}}) \tag{7}$$

The average heat transfer coefficient, h, is obtained from Eq. (8).

$$h = \frac{\dot{Q}}{A_{\mathrm{s}}(T_{\mathrm{b}} - T_{\mathrm{w}})} \tag{8}$$

where the surface area (A_{s}), the bulk temperature ($T_{\mathrm{b}} = (T_{\mathrm{in}} + T_{\mathrm{out}})/2$), and the wall temperature (T_{w}). Utilizing nine T-type thermocouples to measure the radiator wall at different positions will yield the average wall temperature (T_{w}) in Eq. (8).

Uncertainty analysis

In experiments, mistakes can be caused by the apparatus used, the person doing the experiment, or the machine itself. Kline and McClintock [37] first introduced the uncertainty analysis technique, which aims to analyze any mistakes that may occur during the experiments and demonstrate the validity of the data acquired.

Assume that figuring out the magnitude of R is a need for each experimental setting. If one chooses n independent elements ($x_1, x_2, \ldots, x_{\mathrm{n}}$) that influence this size, then R may be written as follows:

$$R = f(x_1, x_2, \ldots., x_{\mathrm{n}}) \tag{12}$$

The fixed error level for each effective independent variable in an experiment is $w_{\mathrm{x1}}, w_{\mathrm{x2}}, \ldots, w_{\mathrm{xn}}$. The experimental inaccuracy of R is given as

$$W_{\mathrm{R}} = \left\{ \left(w_1 \frac{\partial R}{\partial x_1} \right)^2 + \left(w_2 \frac{\partial R}{\partial x_2} \right)^2 + \cdots + \left(w_{\mathrm{n}} \frac{\partial R}{\partial x_{\mathrm{n}}} \right)^2 \right\}^{1/2} \tag{13}$$

The uncertainty in each of the necessary parameters was computed using the approach that Holman [38] suggested. Metrics such as heat transfer rate, heat transfer coefficient, and Nusselt number have estimated uncertainty of 4%, 5.5%, and 6%, respectively.

Results and discussion

This section will present the impacts of several factors, including Reynolds number, φ, and inlet temperature, on both heat transfer and pressure drop. The investigations employed four different MgO nanoparticle volume-based percentages—0.0125%, 0.025%, 0.05%, and 0.1%—as well as pure water (0%), all of which are often used in the literature. While the fluid inlet temperatures were chosen as 40, 50, 60, 70, and 80 °C to correspond with actual conditions, the flow rate was chosen as 5, 8, and 11 Liters per minute (LPM) based on the radiator's capacity.

Effect on Reynolds number (Re)

The Reynolds number, a dimensionless metric, is used to classify fluid systems in which viscosity has a substantial impact on the flow regime. The Reynolds number for a single OSF channel inside the HE is shown in Fig. 6 for three different volume flow rates, various inlet temperatures, and φ values.

With the increase in MgO nanoparticle concentration, the Reynolds number increased up to a critical value and then remained almost constant or started to decrease. For MgO nanoparticle, φ of 0.025% can be considered critical. With the addition of MgO nanoparticles at all temperatures and flow rates, the Reynolds number increased and reached its maximum value up to $\varphi = 0.025\%$. However, after this critical value, the increase in viscous forces overpowered the increase in inertial forces, causing a decrease in the Reynolds number or causing it to remain constant with an approximately equal effect. The increase in inlet temperature caused the viscosity to decrease and the Reynolds number to increase [39, 40]. With the increase in the pump stage, the flow rate increased, and the Reynolds number increased as expected.

Effect on heat transfer rate ($\dot{Q}$)

The heat transfer rate for different fluid inlet temperatures and flow rates for MgO concentrations of 0% (pure water), 0.0125%, 0.025%, 0.05%, and 0.1% are shown in Fig. 7. The heat released from the nanofluid generally increases until $\varphi = 0.025\%$ and then drops for all volumetric flow rates and inlet temperature values. Therefore, it may be concluded that the breaking point is 0.025%. Heat transfer rate is generally seen to increase in tandem with increases in volumetric flow rate and inlet temperature.

At an inlet temperature of 40 °C, the heat transfer rates for $\varphi = 0\%$ and $\varphi = 0.025\%$ are 365.41 W and 499.14 W, respectively, when the refrigerant flow rate is 5 LPM. When the

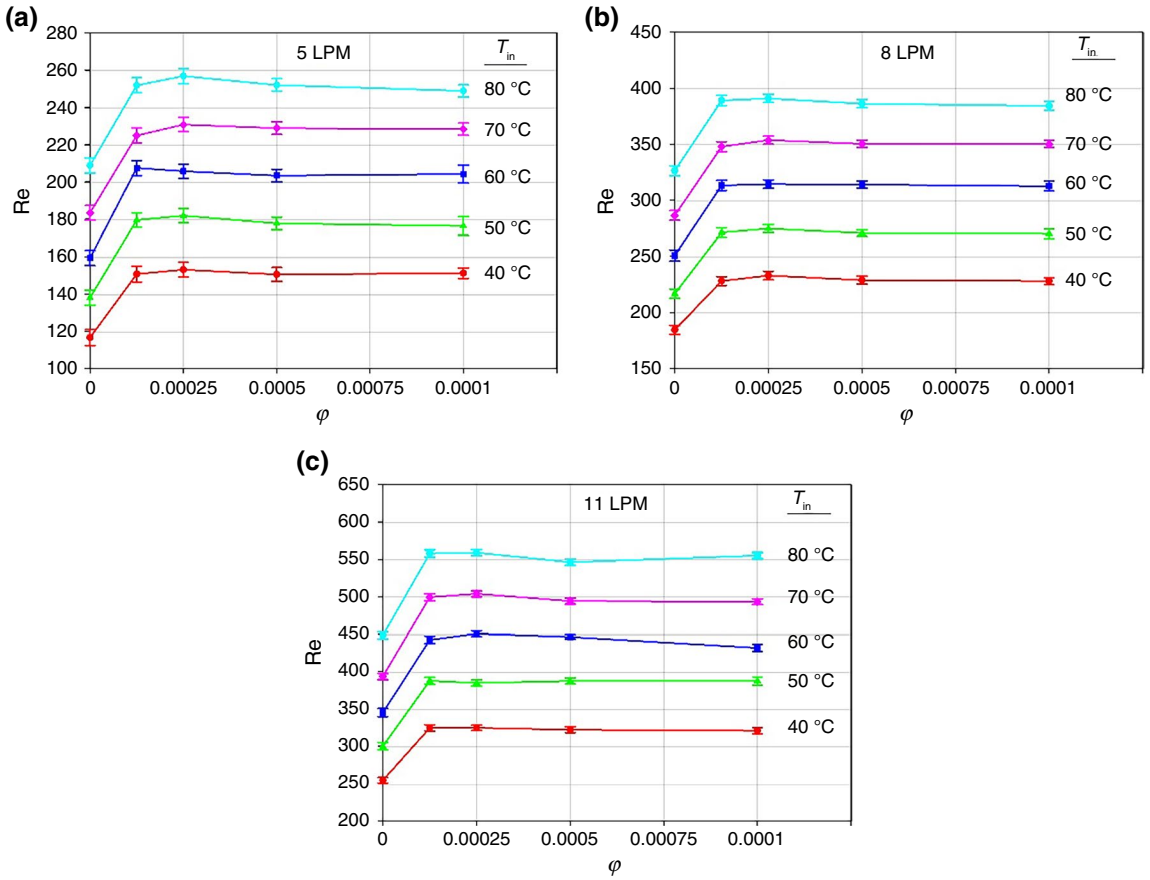


Fig. 6 Variations in the Reynolds number at various volume flow rates, inlet temperatures, and φ values

inlet temperature reaches a maximum of 80 °C, these figures are 1884.41 W and 1776.87 W. In other words, an increase of 36.60% was attained at the 40 °C inlet temperature; however, this figure was only realized at 6.05% when the 80 °C inlet temperature was reached. When the refrigerant flow rate increased to 11 LPM at 40 °C inlet temperature, the heat transfer rates for $\varphi = 0\%$ and $\varphi = 0.025\%$ were 524.78 W and 625 W, respectively, while at 80 °C inlet temperature, the values were 2085.50 W and 2270.96 W. In other words, the value grew to 8.9% when the inlet temperature reached 80 °C, even though an increase of 19.1% was attained at 40 °C.

Heat transfer rates begin to decline sharply as the nanoparticle φ is increased from 0.025 to 0.05% and then to 0.1%. This decrease in heat transfer rate can be demonstrated by increasing the fluid's nanoparticle content. A larger and denser thermal barrier layer forms inside the radiator's OSF channels as a result of the increasing density and viscosity of the nanofluid due to the growing amount of nanoparticles. This results in significant wall shear stress [41–44]. Based on observations, the heat transfer rate is slowed down by the larger and denser boundary layer that forms when the φ of MgO surpasses 0.025%. The Reynolds numbers in Fig. 6 show that the fluid behaves laminarly. Laminar flow is more affected by viscosity than turbulent flow [45]. In light of this, the quantity of nanoparticles utilized and the viscosity rise are critical factors. Brownian motion results from the nanoparticles colliding too frequently with one another as viscosity increases. Brownian motions in nanofluids are explained by the following: chaotic kinematic behavior of nanoparticles in a base fluid that results in increased thermal energy transport with increased thermal conductivity; microconvection phenomena surrounding the particles; and solid-to-solid heat transport resulting from particle collisions and motions [46, 47]. Even while two particles colliding increase the total thermal conductivity (k_{eff}), certain studies in the literature [48, 49] have shown that Brownian motion does not add much to heat conduction. Put differently, above a certain φ level, viscosity increases more quickly than heat conductivity. Moreover, the high particle φ in the base fluid reduces stability and increases the likelihood of agglomeration. As a result of this instability, nanoparticles precipitate [50]. In summary, the heat transfer rate is directly influenced by thermal conductivity and is inversely correlated with the viscosity of the nanofluids. At relatively low φ values, thermal conductivity becomes prominent and improves

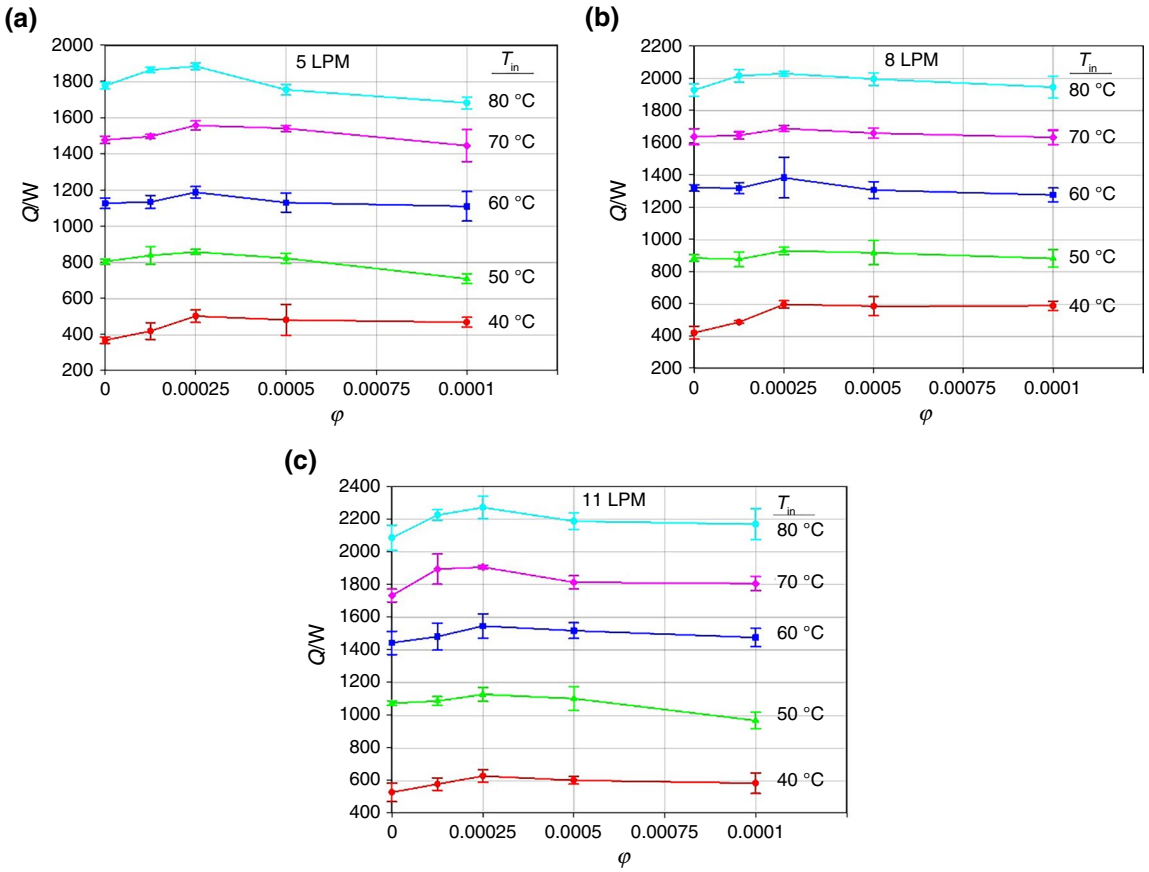


Fig. 7 Variations in the heat transfer rate at various volume flow rates, inlet temperatures, and φ values

heat transmission; at larger φ values, on the other hand, agglomeration of nanoparticles causes viscous phenomena to become prominent. The results show that while specific heat capacity drops, thermal conductivity, density, and dynamic viscosity rise between φ values of 0 and 0.025%. To be more precise, thermal diffusivity rose as a result of more heat being transported overall than being stored. As a result, the φ value rose between 0 and 0.025% for the heat transfer rate. When the φ value exceeded 0.025%, however, agglomeration resulted in a decrease in thermal conductivity while dynamic viscosity increased even more. Consequently, the heat transfer rate started to decrease after this φ value. A specific level of nanoparticle φ value has been identified in various research in the literature to reduce the rate of heat transfer [41, 43, 50].

Effect on heat transfer coefficient (*h*)

The heat transfer coefficient of MgO at different inlet temperatures and volumetric flow rates at volume concentrations of 0.0125%, 0.025%, 0.05%, and 0.1% is shown in Fig. 8. As can be noticed in the figure, the heat transfer coefficient falls at all flow rates and inlet temperature values after increasing as φ rises to the critical value of 0.025%, just like the heat transfer rate does.

It is clear from Fig. 8 that the heat transfer coefficient is directly correlated with the inlet temperature and volumetric flow rate. The heat transfer coefficients at an inlet temperature of 40 °C for $\varphi = 0\%$ and $\varphi = 0.025\%$ are 139.54 $W{\cdot}m^{-2}{\cdot}K^{-1}$ and 397.3 $W{\cdot}m^{-2}{\cdot}K^{-1}$, respectively, when the fluid flow rate is 5 LPM. Nevertheless, they become 479.74 $W{\cdot}m^{-2}{\cdot}K^{-1}$ and 489.83 $W{\cdot}m^{-2}{\cdot}K^{-1}$ when the inlet temperature reaches 80 °C. Put differently, at 40 °C input temperature, the heat transfer coefficient increased by 184.72%, but at 80 °C, this value was 2.10%. Heat transfer coefficients for $\varphi = 0\%$ and $\varphi = 0.025\%$ at 40 °C inlet temperatures are 366.76 $W{\cdot}m^{-2}{\cdot}K^{-1}$ and 621.61 $W{\cdot}m^{-2}{\cdot}K^{-1}$, respectively, when the refrigerant flow rate is increased to 11 LPM. On the other hand, when the inlet temperature rose to 80 °C, the values changed to 579.25 $W{\cdot}m^{-2}{\cdot}K^{-1}$ and 704.72 $W{\cdot}m^{-2}{\cdot}K^{-1}$, respectively. Put differently, the heat transfer coefficient rose by 69.49% at an input temperature of 40 °C, but at 80 °C, this value was 21.66%. There are two reasons why the heat transfer coefficient starts to decrease at a φ of 0.025%. One is that viscosity rises as the particle ratio grows, and the other is that turbulence

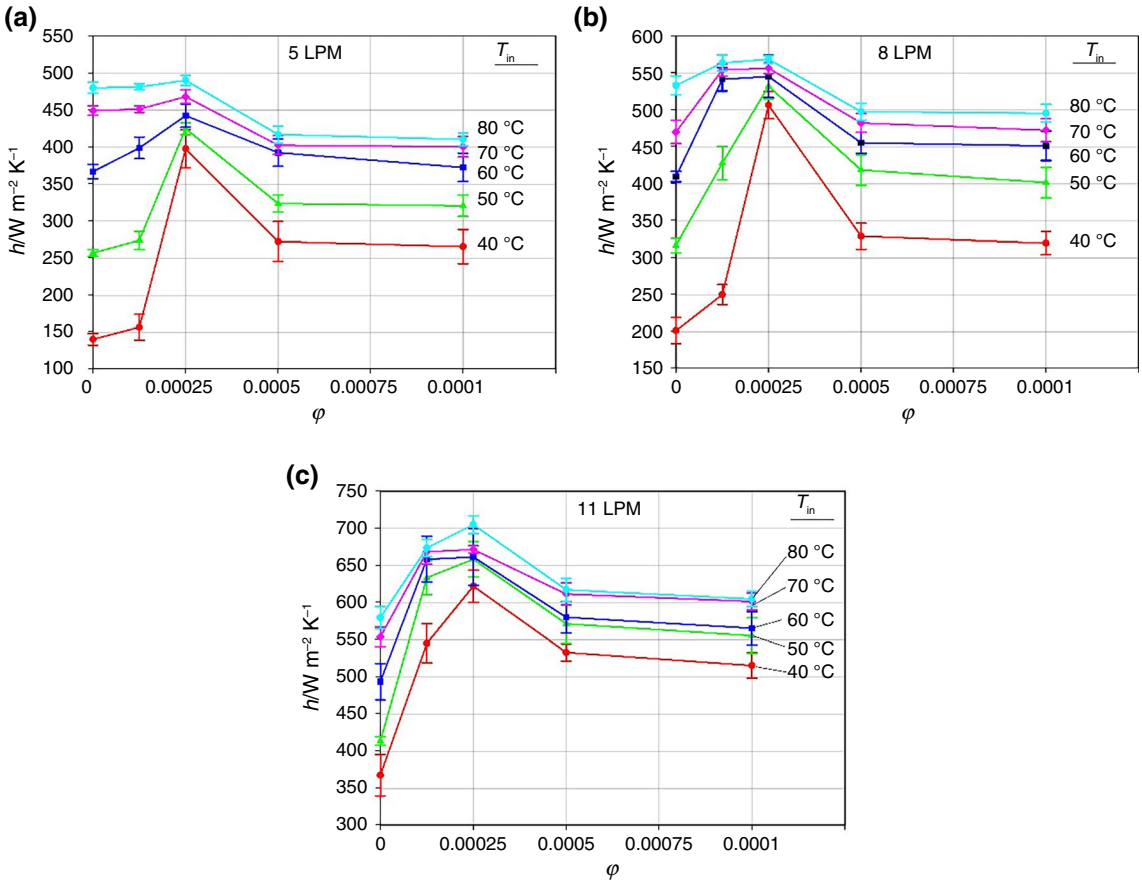


Fig. 8 Variations in heat transfer coefficient at various volume flow rates, inlet temperatures, and φ values

intensity falls as additional nanoparticles increase. The addition of nanoparticles to pure water produced a nanofluid that had a marginally greater thermal conductivity than the base fluid, but not enough to counteract the previously observed decrease in thermal conductivity beyond the critical limit [51]. There have been previous studies [50, 52] in the literature where the heat transfer coefficient was found to have a critical φ value. Taking into account the critical nanoparticle concentration ($\varphi = 0.025\%$), in the case of 40 °C inlet temperature, an increase in flow rate led to an increase in the heat transfer coefficient. This behavior can be attributed to the influence of Reynolds number on the thickness of the thermal boundary layer. As the thickness of the thermal boundary layer rises, the resistance to heat transfer increases. On the other hand, an increase in the Reynolds number leads to a reduction in the thickness of the thermal boundary layer, hence enhancing the heat transfer coefficient. The use of OSFs amplifies this effect by periodically interrupting the thermal boundary layer. At the critical nanoparticle volume concentration ($\varphi = 0.025\%$), the Re number reaches its highest value, indicating that both mechanisms contribute to the enhancement of the heat transfer coefficient.

Effect on Nusselt number (Nu)

In Fig. 9 shows the variation of the Nusselt number at different volumetric flow rates and inlet temperatures for MgO nanoparticle concentrations at 0% (pure water), 0.0125%, 0.025%, 0.05% and 0.1% volumes. It shows that the Nusselt number obtained in this study increases when increasing the MgO nanoparticle concentration from zero (pure water) to 0.025%, and then the Nusselt number generally decreases with increasing MgO nanoparticle concentration. However, the Nusselt number increased with the increase in inlet temperature and flow rate, similar to the situations in heat transfer rate and heat transfer coefficient.

The Nusselt numbers for $\varphi = 0\%$ and $\varphi = 0.025\%$ at 40 °C inlet temperature are 12.17 and 34.62, respectively, at 5 LPM fluid flow rate; as the inlet temperature rises to 80 °C, these values become 39.4 and 39.67. That is to say, the Nusselt number increased by 184.47% at an inlet temperature of 40 °C, but at 80 °C, this value was 0.69%. The Nusselt numbers for $\varphi = 0\%$ and $\varphi = 0.05\%$ at 40 °C inlet temperature become 31.97 and 54, respectively, when the fluid flow rate rose to 11 LPM; however, these values have changed to 47.47, and 57.69 when the inlet temperature is raised to

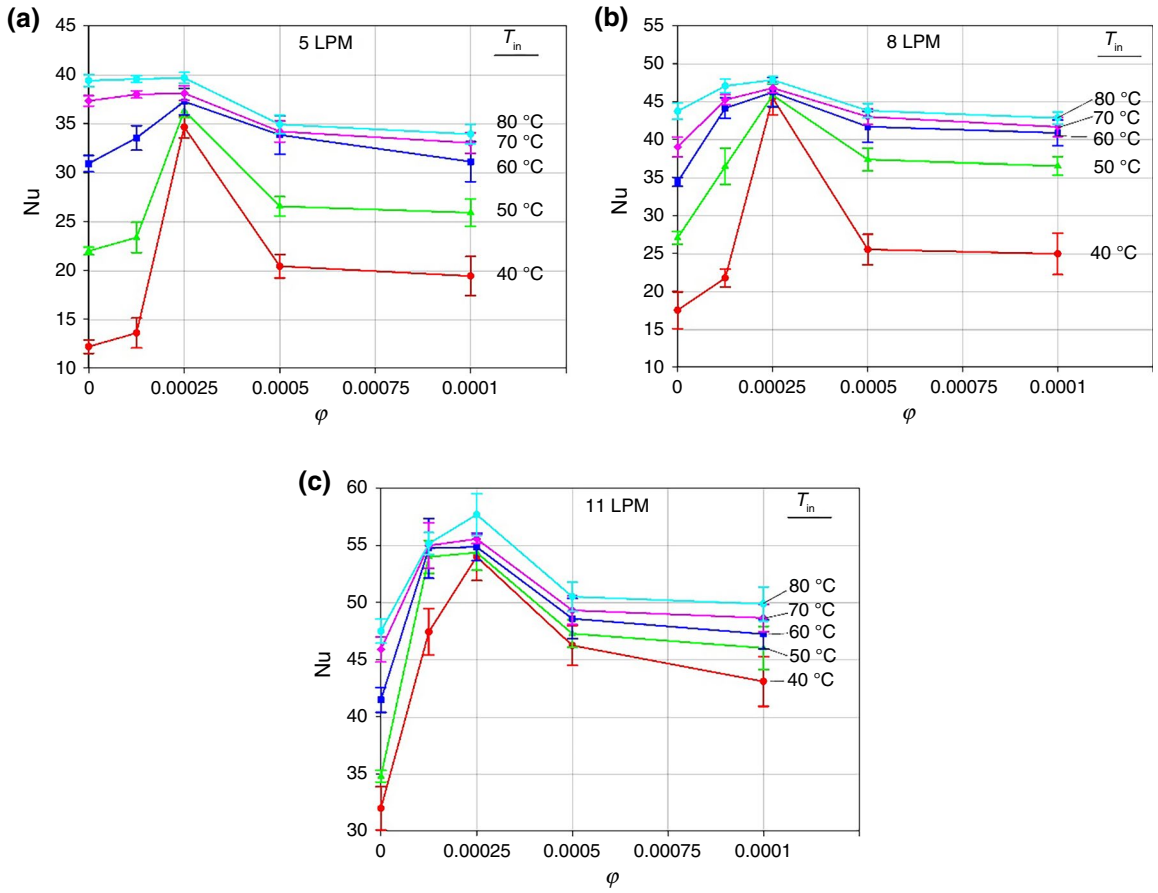


Fig. 9 Variations in the Nusselt number at various volume flow rates, inlet temperatures, and φ values

80 °C. Put differently, at 40 °C inlet temperature, the Nusselt number increased by 68.91%, but at 80 °C, this value increased by 21.53%. Agglomeration may happen in circumstances similar to this study's, when the nanofluid is moving slowly and does not show turbulence, as the φ of nanoparticles increases. Moreover, at relatively large φ values, there might be a decrease in particle velocity and an increase in the effective diameters of overlapping particles, which would slow the rate of heat transfer. Consequently, at low Reynolds numbers, as this study has demonstrated, increasing φ might not improve thermal performance. If the flow is turbulent, different results can be observed [53]. There are other literature studies [43, 52, 53] where an optimum value for the Nusselt number was observed in an examined φ range.

Effect on pressure drop (ΔP)

Figure 10 depicts the variation in the pressure drop for MgO nanoparticle concentrations at 0% (pure water), 0.0125%, 0.025%, 0.05%, and 0.1% volumes at different volumetric flow rates and inlet temperatures.

The data indicates that the pressure drop consistently escalates with the φ. The pressure drop is directly related to the flow rate and inversely proportional to the inlet temperature. The necessary pumping power decreases as the particle concentration of nanofluids grows, but the pressure loss increases as well since less volumetric flow is required to convey the same amount of heat [54]. The high thermal performance of the OSF is due to the large surface area in contact with the fluid and the fact that it provides maximum benefit by preventing fully developed flow in the fluid flow direction for a long time compared to continuous fin geometries. The effect of multiple thermal entrance lengths aroused by repetition in the thermal boundary layer in the fluid flow direction and the generation of oscillatory velocity resulting from left–right collisions of the fluid allows the heat transfer coefficient and, thus, the heat transfer rate to increase. [32, 39, 55]. Velocity boundary layer thickness is lowest, and wall shear stress is highest in the entrance region. As a result, the inflow region has a large pressure drop. As the wall shear stress falls in a fully developed zone, the thickness of the velocity boundary layer increases. Viscosity and wall shear stress both rise in tandem with an increase in

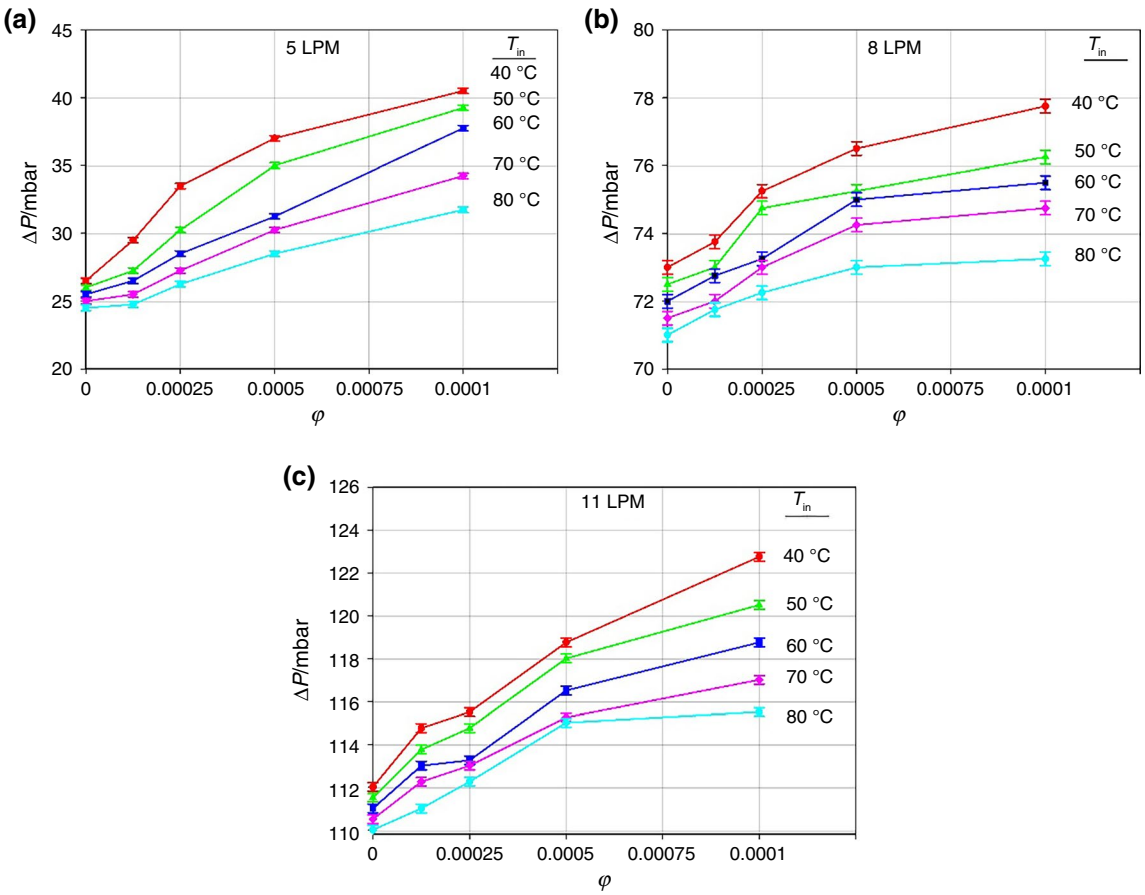


Fig. 10 Variations in the Pressure drop (ΔP) at various volume flow rates, inlet temperatures, and φ values

nanoparticle volume concentration. When nanoparticles are added, the nanofluid's viscosity rises, which in turn causes the wall shear stress to rise. As a result, the pressure drop rises, and velocity boundary layer thickness decreases [39, 56].

Conclusions

Plate-fin heat exchangers are almost inevitable to utilize for increased heat transfer efficiency applications. One of these applications is automobile radiators in which high efficiency and compactness are desired. Although this type of heat exchangers can provide high efficiency, it can be more improved by utilizing the nanofluids as coolant. For this purpose, MgO–pure water nanofluid has been utilized as coolant with different φ values (0%, 0.025%, 0.05%, 0.1% and 0.2%) and its effect on both thermal and hydrodynamic performance has been investigated with respect to different coolant temperatures and flow rate. As a result of this study following conclusions are obtained:

- The effect of different φ values of on the Re number at different inlet temperatures has been observed and it has been concluded that for a given volume flow rate Re number has increased and reached its maximum value for the φ of 0.025%, then it decreased and remained constant. This behavior is observed for any given inlet temperatures and can be attributed to increasing dynamic viscosity and density of the nanofluid by increasing φ has resulted in constant Re number within the φ range of 0.00025–0.001.
- Increasing the volume flow rate has increased the Re number for a given φ and inlet temperature as expected. Also it is observed that for a given φ and volume flow rate, Re number increases with increasing inlet temperature. This can be explained by decrease in dynamic viscosity is more dominant than the decrease in density as the temperature rises.
- The heat transfer rate for a given φ, inlet temperature and volume flow rate has been investigated and it has been observed that the heat transfer rate has a critical value of φ which is 0.025%. Since at the critical value of φ Re

number reaches its maximum value it is an expected heat transfer behavior.

- For a given φ, the heat transfer rate increases with increasing inlet temperature. For instance, when the φ of nanoparticle is at its critical value (0.025%) and the volume flow rate is 11 LPM, the heat transfer rate increases about 265% when the inlet temperature changes from 40 to 80 °C. This behavior can be attributed to change in Re number from 325 to 560 for 40 °C and 80 °C conditions, respectively.
- The heat transfer coefficient and Nu number behavior follow the same characteristics for a given inlet temperature, volume flow rate and φ since these parameters are firmly related to each other.
- Pressure drops across the heat exchanger have shown a increasing behavior for the higher φ values since the density of the nanofluid increases with higher values of φ. In addition to that, for a given φ, the lower the inlet temperatures have resulted in higher the pressure drop due to the increase in density.

This study investigates the potential of MgO nanofluids in heavy-duty vehicle engine cooling systems by utilizing their superior thermal properties. The use of nanofluids may offer the opportunity to reduce fuel consumption by optimizing the dimensions of engine cooling systems. However, the study encountered limitations such as the tendency to agglomerate at high nanoparticle concentrations and the consequent deterioration in thermal performance. Future research may focus on improved nanofluid production and preparation methods that can minimize agglomeration at higher concentrations. Furthermore, the study of different single and hybrid nanofluids, as well as the effects of higher fluid inlet temperatures and flow rates, is suggested for the extension of the research.

Acknowledgements This research has received financing from the Gazi University Scientific Research Projects Coordination Unit, Grant Number FKB-2022-7523. We express our gratitude for their assistance. We extend our gratitude to Prof. Dr. Hamit SOLMAZ and Prof. Dr. Zeki YILMAZOĞLU for providing the equipment utilized in our research.

Funding Open access funding provided by the Scientific and Technological Research Council of Türkiye (TÜBİTAK).

Open Access This article is licensed under a Creative Commons Attribution 4.0 International License, which permits use, sharing, adaptation, distribution and reproduction in any medium or format, as long as you give appropriate credit to the original author(s) and the source, provide a link to the Creative Commons licence, and indicate if changes were made. The images or other third party material in this article are included in the article's Creative Commons licence, unless indicated otherwise in a credit line to the material. If material is not included in the article's Creative Commons licence and your intended use is not permitted by statutory regulation or exceeds the permitted use, you will need to obtain permission directly from the copyright holder. To view a copy of this licence, visit http://creativecommons.org/licenses/by/4.0/.

References

1. Kays WM, London AL. Compact heat exchangers. New York: McGraw-Hill; 1984.
2. Sözen A, Khanları A, Çiftçi E. Experimental and numerical investigation of nanofluid usage in a plate heat exchanger for performance improvement. Int J Renew Energy Dev. 2019;8(1):27–32. https://doi.org/10.14710/ijred.8.1.27-32.
3. Morteza K-A, Mortazavi S. Combined effects of holes and winglets on chevron plate-fins to enhance the performance of a plate-fin heat exchanger working with nanofluid. Exp Heat Transf. 2019;32(6):584–99. https://doi.org/10.1080/08916152.2019.1569176.
4. Yang Y, Li S, Liu H. Experimental investigation on the heat transfer behavior of water in offset strip fin channels. Int J Heat Mass Transf. 2023;202:123656. https://doi.org/10.1016/j.ijheatmasstransfer.2022.123656.
5. Blecich P, Batista J, Kirinčić M, Trp A, Lenić K. Numerical study of heat transfer and fluid flow in the offset strip-fin heat exchanger: a fin-by-fin analysis. Int Commun Heat Mass Transf. 2024;154:107464. https://doi.org/10.1016/j.icheatmasstransfer.2024.107434.
6. Xiang H, Du W, Zhao J. Numerical investigation on the thermal-hydraulic performance of high Prandtl number fluid in offset strip fin with different offset. Int J Heat Mass Transf. 2024;220:124915. https://doi.org/10.1016/j.ijheatmasstransfer.2023.124915.
7. Elibol EA. Performance analysis of a refrigeration system integrated with a thermoelectric cooler and microchannels in terms of heat transfer using a hybrid nanofluid. Appl Therm Eng. 2024;250:123465.
8. Choudhary S, Sachdeva A, Kumar P. Investigation of the stability of MgO nanofluid and its effect on the thermal performance of flat plate solar collector. Renewable Energy. 2020;147:1801–14.
9. Elibol EA, Yilmazoglu MZ, Aksoy AE, Aktas F. Thermal analysis of a refrigeration system integrated with a thermoelectric couple and microchannels using TiO_2–water nanofluid. Int J Heat Fluid Flow. 2024;108:109491.
10. Li Z, et al. Numerical assessment on the hydrothermal behavior and irreversibility of MgO–Ag/water hybrid nanofluid flow through a sinusoidal hairpin heat-exchanger. Int Commun Heat Mass Transf. 2020;115:104628.
11. Choi S. Enhancing thermal conductivity of fluids with nanoparticles. In: Siginer DA, Wang HP, editors. Developments applications of non-newtonian flows, FED-vol 231/MD-vol 66. New York: ASME; 1995. p. 99–105.
12. Khoshvaght-Aliabadi M, Salami M. Turbulent flow of Al_2O_3–water nanofluid through plate-fin heat exchanger (PFHE) with offset-strip channels. Therm Sci Eng Prog. 2018;6:164–76. https://doi.org/10.1016/j.tsep.2018.04.001.
13. Kumar A, Chand P, Hassan MA. Louvered finned car radiator with MWCNT-SiO_2 hybrid nanofluid: an experimental approach. Powder Technol. 2023;415:118176. https://doi.org/10.1016/j.powtec.2022.118176.
14. Karana DR, Sahoo RR. Effect on TEG performance for waste heat recovery of automobiles using MgO and ZnO nanofluid coolants. Case Stud Therm Eng. 2018;12:358–64. https://doi.org/10.1016/j.csite.2018.05.006.
15. Rai PK, Kumar A, Yadav A. Experimental investigation of heat transfer augmentation in automobile radiators using magnesium

oxide/distilled water-ethylene glycol based nanofluid. Mater Today Proc. 2018;24:1525–32.
16. Ali HM, Azhar MD, Saleem M, Saeed QS, Saieed A. Heat transfer enhancement of car radiator using aqua based magnesium oxide nanofluids. Therm Sci. 2015;19(6):2039–48. https://doi.org/10.2298/TSCI150526130A.
17. Gamal M, Radwan MS, Elgizawy IG, Shedid MH. Heat transfer performance and exergy analyses of MgO and ZnO nanofluids using water/ethylene glycol mixture as base fluid. Numer Heat Transf A Appl. 2021;80(12):597–616. https://doi.org/10.1080/10407782.2021.1962631.
18. Kadam SV, Mohite SS, Kumbhar VS. Heat transfer enhancement by the usage of low concentration MgO–water nanofluid. Int J Eng Adv Technol. 2019;9(1):1985–90. https://doi.org/10.35940/ijeat.A9528.109119.
19. Qusay HKH, Al-Amir R. Experimental investigation to heat transfer augmentation in a car radiator worked with water–magnesium oxide nanofluid. J Babylon Univ/Eng Sci. 2017;4(25):1179–93.
20. Li Z, Shahsavar A, Niazi K, Al-Rashed AA, Rostami S. Numerical assessment on the hydrothermal behavior and irreversibility of MgO–Ag/water hybrid nanofluid flow through a sinusoidal hairpin heat-exchanger. Int Commun Heat Mass Transf. 2020;115:104628.
21. Jasim DJ, Karouei SH, Mohammed TJ, Al-Shati AS. Hydrothermal behaviour of hybrid nanofluid flow in two types of shell and helical coil tube heat exchangers with a new design; Numerical approach. Int J Thermofluids. 2024;24:100902.
22. Azizi HZ, Shokri V, Karouei SHH. Hydrothermal behaviour of hybrid nanofluid flow in a shell-and conical coil tube heat exchanger; numerical approach. Case Stud Therm Eng. 2024;58:104435.
23. Colangelo G, et al. Numerical evaluation of a HVAC system based on a high-performance heat transfer fluid. Energies. 2021;14(11):3298.
24. Milanese M, et al. Experimental evaluation of a full-scale HVAC system working with nanofluid. Energies. 2022;15(8):2902.
25. Colangelo G, et al. Thermal conductivity, viscosity and stability of Al_2O_3-diathermic oil nanofluids for solar energy systems. Energy. 2016;95:124–36.
26. Iacobazzi F, et al. A critical analysis of clustering phenomenon in Al_2O_3 nanofluids. J Therm Anal Calorim. 2019;135(1):371–7.
27. Babat RAA, et al. Experimental study on the utilization of magnetic nanofluids in an air-to-air heat pipe heat exchanger. Chem Eng Commun. 2021;210(5):687–97.
28. Çiftçi E, Martin K, Sözen A. Enhancement of thermal performance of the air-to-air heat pipe heat exchanger (AAHX) with aluminate spinel-based binary hybrid nanofluids. Heat Trans Res. 2021;52(17):81.
29. Goudarzi K, Jamali H. Heat transfer enhancement of Al_2O_3-EG nanofluid in a car radiator with wire coil inserts. Appl Therm Eng. 2017;118:510–7.
30. Mahbubul I, et al. Optimization of ultrasonication period for better dispersion and stability of TiO_2–water nanofluid. Ultrason Sonochem. 2017;37:360–7.
31. Huang J. Research on high water temperature of diesel engine and improvement of radiator. In: 2nd International conference on advances in mechanical engineering and industrial informatics (AMEII 2016). 2016. https://doi.org/10.2991/AMEII-16.2016.15
32. Elibol EA, Turgut O. Heat transfer and fluid flow characteristics in a long offset strip fin channel by using TiO_2–water nanofluid. Arab J Sci Eng. 2022;47:15415–28.
33. Khanafer K, Vafai K. A critical synthesis of thermophysical characteristics of nanofluids. Int J Heat Mass Trans. 2011;54(19–20):4410–28.
34. Mackolil J, Mahanthesh B. Heat transfer optimization and sensitivity analysis of Marangoni convection in nanoliquid with nanoparticle interfacial layer and cross-diffusion effects. Int Commun Heat Mass Transf. 2021;126:105361.
35. Maxwell JC. A treatise on electricity and magnetism, vol. 314. Oxford: Clarendon; 1881. p. 1873.
36. Corcione M. Heat transfer features of buoyancy-driven nanofluids inside rectangular enclosures differentially heated at the sidewalls. Int J Therm Sci. 2010;49(9):1536–46.
37. Kine S, McClintock F. Describing uncertainties in single-sample experiments. Mech Eng. 1953;75:3–8.
38. Holman JP. Experimental methods for engineers. 2012.
39. Elibol EA, Turgut O, Aktas F, Senol H, Celik AF. Experimental investigation on heat transfer and flow characteristics of TiO_2–water nanofluid in a heavy vehicle radiator. J Therm Anal Calorim. 2022;148:977–94. https://doi.org/10.1007/s10973-022-11817-3.
40. Ahmed SA, Ozkaymak M, Sözen A, Menlik T, Fahed A. Improving car radiator performance by using TiO_2–water nanofluid. Eng Sci Technol an Int J. 2018;21:996–1005. https://doi.org/10.1016/j.jestch.2018.07.008.
41. Ali HM, Ali H, Liaquat H, Bin Maqsood HT, Nadir MA. Experimental investigation of convective heat transfer augmentation for car radiator using ZnO–water nanofluids. Energy. 2015;84:317–24. https://doi.org/10.1016/j.energy.2015.02.103.
42. Zhou XR, Wang Y, Zheng K, Huang H. Comparison of heat transfer performance of ZnO-PG, α-Al_2O_3-PG, and γ-Al_2O_3-PG nanofluids in car radiator. Nanomater Nanotechnol. 2019;9:1–12. https://doi.org/10.1177/1847980419876465.
43. Qasim M, Sajid Kamran M, Ammar M, Ali Jamal M, Yasar JM. Heat transfer enhancement of an automobile engine radiator using ZnO water base nanofluids. J Therm Sci. 2020;29:1010–24. https://doi.org/10.1007/s11630-020-1263-9.
44. Ni K, Fang H, Yu Z, Fan Z. The velocity dependence of viscosity of flowing water. J Mol Liq. 2019;278:234–8. https://doi.org/10.1016/j.molliq.2019.01.055.
45. Milanese M, Iacobazzi F, Colangelo G, de Risi A. An investigation of layering phenomenon at the liquid–solid interface in Cu and CuO based nanofluids. Int J Heat Mass Transf. 2016;103:564–71. https://doi.org/10.1016/j.ijheatmasstransfer.2016.07.082.
46. Iacobazzi F, Milanese M, Colangelo G, Lomascolo M, de Risi A. An explanation of the Al_2O_3 nanofluid thermal conductivity based on the phonon theory of liquid. Energy. 2016;116:786–94. https://doi.org/10.1016/j.energy.2016.10.027.
47. Wang X, Xu X, Choi SUS. Thermal conductivity of nanoparticle-fluid mixture. J Thermophys Heat Transf. 1999;13:474–80. https://doi.org/10.2514/2.6486.
48. Keblinski P, Phillpot SR, Choi SUS, Eastman JA. Mechanisms of heat flow in suspensions of nano-sized particles (nanofluids). Int J Heat Mass Transf. 2002;45:855–63. https://doi.org/10.1016/S0017-9310(01)00175-2.
49. Dey D, Sahu DS. A review on the application of the nanofluids. Heat Transf. 2021;50:1113–55. https://doi.org/10.1002/htj.21920.
50. Ali M, El-Leathy AM, Al-Sofyany Z. The effect of nanofluid concentration on the cooling system of vehicles radiator. Adv Mech Eng. 2014;2014:1–13. https://doi.org/10.1155/2014/962510.
51. Huang D, Wu Z, Sunden B. Pressure drop and convective heat transfer of Al_2O_3/water and MWCNT/water nanofluids in a chevron plate heat exchanger. Int J Heat Mass Transf. 2015;89:620–6. https://doi.org/10.1016/j.ijheatmasstransfer.2015.05.082.
52. Zhong D, Zhong H, Wen T. Investigation on the thermal properties, heat transfer and flow performance of a highly

self-dispersion TiO_2 nanofluid in a multiport mini channel. Int Commun Heat Mass Transf. 2020;117:104783. https://doi.org/10.1016/j.icheatmasstransfer.2020.104783.
53. Tafakhori M, Kalantari D, Biparva P, Peyghambarzadeh SM. Assessment of Fe_3O_4–water nanofluid for enhancing laminar convective heat transfer in a car radiator. J Therm Anal Calorim. 2021;146:841–53. https://doi.org/10.1007/s10973-020-10034-0.
54. Vajjha RS, Das DK, Namburu PK. Numerical study of fluid dynamic and heat transfer performance of Al_2O_3 and CuO nanofluids in the flat tubes of a radiator. Int J Heat Fluid Flow. 2010;31:613–21. https://doi.org/10.1016/j.ijheatfluidflow.2010.02.016.
55. Elibol EA, Turgut O. Thermal-hydraulic performance of tio2-water nanofluids in an offset strip fin heat exchanger. Therm Sci. 2022;26(1):553–65. https://doi.org/10.2298/TSCI201019063E.
56. Elibol EA, Gonulacar YE, Aktas F, Tigli B. Effect of using a ZnO-TiO_2/water hybrid nanofluid on heat transfer performance and pressure drop in a flat tube with louvered finned heat exchanger. J Therm Anal Calorim. 2024;149(15):8665–80. https://doi.org/10.1007/s10973-024-13346-7.

Publisher's Note Springer Nature remains neutral with regard to jurisdictional claims in published maps and institutional affiliations.